Biological Tissue Characterization by Magnetic Induction Spectroscopy (MIS): Requirements and Limitations

Hermann Scharfetter*, Roberto Casañas, and Javier Rosell

***Abstract*—Magnetic induction spectroscopy (MIS) aims at the contactless measurement of the passive electrical properties (PEP) σ, ε, and μ of biological tissues via magnetic fields at multiple frequencies. Whereas previous publications focus on either the conductive or the magnetic aspect of inductive measurements, this article provides a synthesis of both concepts by discussing two different applications with the same measurement system: 1) monitoring of brain edema and 2) the estimation of hepatic iron stores in certain pathologies. We derived the equations to estimate the sensitivity of MIS as a function of the PEP of biological objects. The system requirements and possible systematic errors are analyzed for a MIS-channel using a planar gradiometer (PGRAD) as detector. We studied 4 important error sources: 1) moving conductors near the PGRAD; 2) thermal drifts of the PGRAD-parameters; 3) lateral displacements of the PGRAD; and 4) phase drifts in the receiver. All errors were compared with the desirable resolution. All errors affect the detected imaginary part (mainly related to σ) of the measured complex field much less than the real part (mainly related to ε and μ). Hence, the presented technique renders possible the resolution of (patho-) physiological changes of the electrical conductivity when applying highly resolving hardware and elaborate signal processing. Changes of the magnetic permeability and permittivity in biological tissues are more complicated to deal with and may require chopping techniques, e.g., periodic movement of the object.**

***Index Terms*—Brain edema, impedance spectroscopy, iron overload, magnetic induction tomograpy, passive electrical properties of tissue.**

I. Introduction

A. Measurement Principle

MEASUREMENT of the passive electrical properties (PEP) of biological tissues form the basis of several noninvasive diagnostic methods which are also suitable for online monitoring of organ function in the human body. All related measurement methods apply an electromagnetic excitation field and measure the object's response field. Characteristically they operate in the near field of the excitation source. Typical applications are e.g., body impedance analysis, tissue hydration measurement, monitoring of cardiac function (stroke volume estimation), monitoring of lung function, detection of malignant tissue, etc. [1]. A general trend found in all this techniques is the use of multiple frequencies trying to increase the accuracy and the diagnostic capability.

In the field of biomedicine, the most important PEP are the electrical conductivity σ and the dielectric permittivity ε, but also the magnetic permeability μ can be of diagnostic interest (see Section I-C). Practically all established measurement methods of PEP require the connection of the patients via electrodes in order to inject weak alternating electrical currents and to measure the potential differences across determined sensing electrodes. The diagnostic information is extracted from the corresponding transimpedances of the segment under investigation (bioimpedance methods). Measurements with a certain spatial resolution can be obtained with multichannel methods, i.e., electrical impedance tomography (EIT).

All bioimpedance electrode-based methods suffer from the following drawbacks.

- The electrodes introduce measurement errors due to the poorly defined electrode–skin interface.
- The accuracy of absolute or static image reconstruction methods for EIT depends critically on the exact knowledge of the electrode locations. This requirement is difficult to fulfil because of the variability of the body surface geometry.
- Intracranial applications are difficult to perform in adults due to the high resistivity of the skull.

If the latter restriction could be obviated, monitoring of the PEP would represent a valuable tool for applications in the central nervous system, as suggested previously, e.g., for the early detection of brain edema by monitoring of the conductivity [2], [3]. Other intracranial applications so far suggested refer to the monitoring of ventricular hemorrhage [4], [5], stroke, the evolution of spreading depressions, and epilepsy [6].

A promising alternative to some electrode-based methods is magnetic induction spectroscopy (MIS) [7], [8]. This new technique is a multifrequency version of the recently developed magnetic induction tomography (MIT) [9], [10]. MIS requires an alternating magnetic excitation field $\mathbf{B_0}$ which is coupled from an excitation coil (EXC) to the object under investigation (see Fig. 1). Changes $\Delta\kappa$ of the complex conductivity $\kappa = \sigma + j\omega\varepsilon_0\varepsilon_r$ and changes $\Delta\mu_r$ of the relative magnetic

Manuscript received June 4, 2002; revised December 15, 2002. This work was supported by the Austrian Science Foundation FWF, Project P14990, by the Spanish MCYT, Project SAF-2001-1660-C02, and by the Integrated Action/Accion Integrada Spain-Austria HU00-16 and 14/2001. *Asterisk indicates corresponding author.*

*H. Scharfetter is with the Institute for Biomedical Engineering, Graz University of Technology, Inffeldgasse 18, A-8010 Graz, Austria (e-mail: scharfetter@bmt.tu-graz.ac.at).

R. Casañas is with the Departament d'Enginyeria Electrònica, Universitat Politècnica de Catalunya, 08034 Barcelona, Spain and also with the Escuela de Bioanalisis, Facultad de Medicina, Universidad Central de Venezuela, Caracas, Venezuela (e-mail: robertoc@eel.upc.es).

J. Rosell is with the Escuela de Bioanalisis, Facultad de Medicina, Universidad Central de Venezuela, Caracas, Venezuela (e-mail: jrosell@eel.upc.es).

Digital Object Identifier 10.1109/TBME.2003.813533

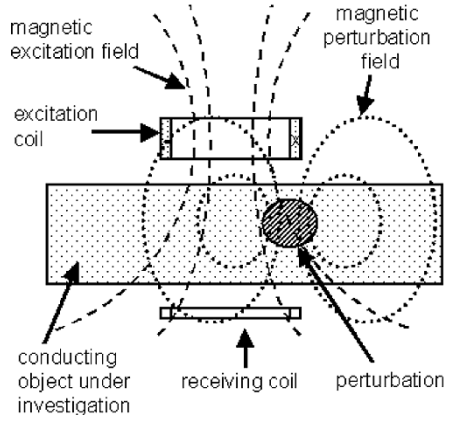

Fig. 1. Principle of magnetic induction spectroscopy. The eddy currents flow in closed loops around the axis of the coils, increasing in current density from the axis toward a maximum the location of which depends on the particular geometry.

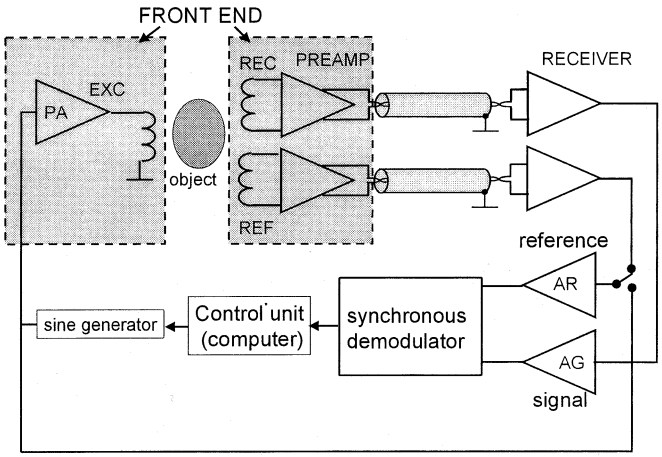

Fig. 2. Single-channel measurement system.

permeability in a target region cause a field perturbation $\Delta\mathbf{B}$ due to the induction of eddy currents and magnetic dipoles in the object under investigation. The perturbation field is then measured via suitable receiver coils.

MIS, in contrast to bioimpedance approaches, offers several advantages.

- It does not require galvanic coupling between the device and the object under measurement, hence avoiding the ill-defined electrode–skin interface.
- The skull does not present a barrier for the magnetic field. Hence, the method is particularly attractive for monitoring in the central nervous system of adults.
- Due to the contactless operation, requirements for electrical safety are easier to fulfil than with electrode-based methods.
- The location of the sensing elements (coils) is always well defined if they are mounted on a rigid support. Hence, the boundary conditions are well reproducible, if the air between the coil system and the body under investigation is included into the target volume of the reconstruction problem.

An additional feature of MIS is its inherent sensitivity to the magnetic permeability μ so that, in contrast to bioimpedance methods, also changes of the magnetic properties of biological matter can be studied. The aim of this article is the detailed analysis of the requirements and limitations of a MIS system for biomedical applications. As examples we studied one application which is based on conductivity changes in the target region and another where changes of μ are of diagnostic interest:

B. Example 1: Brain Edema Monitoring

Unless detected in time, brain edema can lead to life threatening hazards by increasing the intracranial pressure up to values, which cause tissue damage. As reviewed in [3] ischemic states or lesions can be detected from changes in the brain conductivity within minutes whereas in computed tomography (CT) or magnetic resonance imaging (MRI) the first changes appear with a marked delay. Magnetic brain monitoring could, in fact, provide a useful method, as there exists still no noninvasive and continuous instrumentation for the detection of brain edema. This application relies on the fact that water accumulations in tissue cause local changes of the PEP σ and ε, as has been demonstrated with invasive measurements, e.g., in [11] and [12].

C. Example 2: Determination of Excess Iron Stores in Liver Tissue

An interesting biomedical application based on the characterization of magnetic properties in biological tissue is the quantification of hepatic iron overload in cases of hereditary hemochromatosis or in patients subject to periodic blood transfusion. Magnetic induction methods have been tried previously for the characterization of the paramagnetic and diamagnetic properties of biological tissues [13] but the sensitivity is considerably low. To our knowledge, the only noninvasive measurement method so far tested for hepatic iron overload in humans is based on SQUIDs [14], [15] or on MRI [16]. However, also much simpler magnetic sensors are studied to allow the detection of physiological and pathophysiological iron concentrations in human subjects [17], [18].

II. Methods

A. General Measuring System

Fig. 2 shows the principle of a single measuring channel for a MIS system, as published previously in [8], [19]. The excitation coil (EXC) is fed by a power amplifier (PA) with a sinusoidal current. The magnetic field $\mathbf{B_0}$ and its perturbation $\Delta\mathbf{B}$ are picked up in form of voltages V_0 and ΔV, respectively, which are induced in receiver coils (REC). The signal ΔV is decomposed into real and imaginary parts by digital synchronous demodulation. The respective reference signal is derived either directly from the excitation circuit, or, as depicted, from a reference sensor (REF) which detects the main excitation field. The signals from the REC and REF are preconditioned by differential preamplifiers with a differential current output [19]. The amplifiers should be located very close to the coil system in order

to keep phase errors due to long cables as small as possible. The transmission to the mainframe has been realized via twisted pair cables in order to guarantee minimum magnetic interference.

B. Expected Sensitivities

The sensitivity of an inductive measuring system can be expressed as the voltage change ΔV in the receiver coil due to a small change $\Delta\kappa$ and $\Delta\mu$ of the PEP in the space Ω filled with the electromagnetic field. A general expression can be derived from the law of reciprocity for a linear two-port system with ports A and B fed by a current I [20]

$$\Delta V = \frac{1}{I}\left[\Delta\kappa \int_{\Omega} (\nabla\Phi + j\omega A_\Phi)\cdot(\nabla\Psi + j\omega A_\Psi) d\Omega + j\omega\Delta\mu \int_{\Omega} H_\Phi \cdot H_\Psi d\Omega\right] \quad (1)$$

with Φ, A_Φ: electrical scalar potential and magnetic vector potential when feeding the system from port A; Ψ, A_Ψ: electrical scalar potential and magnetic vector potential when feeding the system from port B; H_Φ, H_Ψ: the corresponding magnetic field intensity vectors.

The general solution of this equation requires elaborate numerical methods. For a raw estimation of the expected sensitivities, however, some simple analytical or semi-analytical solutions can be derived for special cases with a simple geometry. For a small object in the empty space, the spatial sensitivity distribution could be approximated with the scalar product of the magnetic fields when feeding the system from port A and B [7]. A more simple, but illustrative closed solution can be obtained for a cylindrical sample with radius R and thickness t $(t \ll 2a)$ positioned coaxially halfway between two small coils with distance $2a$. The relative change of the magnetic field in the receiver coil and, hence, the corresponding relative voltage change can be expressed by (2)

$$\frac{\Delta B}{B_0} = \frac{\Delta V}{V_0} = \frac{a^3 t}{2}\left\{\chi_m \frac{R^2(8a^2 - R^2)}{(a^2+R^2)^4} - j(\sigma + j\omega\varepsilon_0\varepsilon_r)\omega\mu_0 \times \left[\frac{1}{a^2} - \frac{a^2+2R^2}{(a^2+R^2)^2}\right]\right\}$$
$$\kappa = \sigma + j\omega\varepsilon_0\varepsilon_r; \quad and \quad \chi_m = \mu_r - 1 \quad (2)$$

where χ_m denotes the magnetic susceptibility of the material. The second term on the right-hand side of (2) has been derived previously in [21], the first term is derived in Appendix I according to [17]. Equation (2) is valid only for the case of "weak perturbation," i.e., if the alteration of the excitation field by the response field is negligible and if μ_r is close to 1. This is the case for biological objects (conductivity < 2 S/m) up to about 10 MHz. A semi-analytical solution which remains valid also at very low penetration depths has been presented in [8] for a small conducting and paramagnetic sphere located in an arbitrary point between two circular coils. In the following, the key quantity $\Delta V/V_0$ shall be called the "signal/carrier ratio" (SCR) [8]. It is a function of the location $\mathbf{x}$ of the perturbation and of the coil system [7].

From (2), the following important properties of the SCR become obvious.

1) The real part is associated with changes of the relative permeability and permittivity whereas the imaginary part reflects changes of the conductivity σ.
2) The imaginary part is proportional to σ and the radian frequency ω
3) The contribution of the relative permittivity ε_r to the real part of the SCR is proportional to ω^2. Taking into account that the relative permittivity for biological tissue at low frequencies (10 Hz-1 kHz) can be in the range $10^4 - 10^6$ [1], its contribution can be in the same order of magnitude as that of the conductivity, at moderate frequencies.
4) The term associated with χ_m does not depend on the frequency. The dielectric contribution can be neglected at low frequencies (some kilohertz) due to its dependence on ω^2 if the permittivity is not excessively high. Moreover, below a certain frequency, also changes of the imaginary part fall below the noise level of the detectors due to the dependence on ω. In this case, changes of the permeability become entirely predominant in the signal.

C. Application Example 1: Detection of Conductivity Changes $(\chi_m = 0)$

Many tissue properties, especially the hydration state, are well reflected by the frequency-dependence of the conductivity, especially in the range 10 kHz–10 MHz (β-dispersion range, [22]–[24]. The conductivity at low frequencies reflects essentially the extracellular fluid volume whereas with increasing frequency the additional contribution of the intracellular fluid volume causes a significant increase of the conductivity. From previous investigations, e.g., [27] magnetic methods are not expected to work at frequencies lower than 10 kHz due to physical limitations. Hence, the range accessible for MIT will extend from several tens of kHz up to several tens of MHz, the upper limit being determined by the penetration depth of the electromagnetic field and the desired sounding depth. This range covers fairly well the β-dispersion. The SCR is considerably low at the low end of the β-dispersion. According to the semi-analytical model in [8] a conducting sphere in empty space (radius $r = 25$ mm, $\sigma = 1$ S/m and $\varepsilon_r = 80$) positioned halfway on the axis between two coils (35 mm radius, inter-coil distance 250 mm) produces a SCR of $-1.8 \cdot 10^{-10} - j8.9 \cdot 10^{-7}$ at 50 kHz. As analyzed in [19] the sensitivity map for conductive perturbations embedded in a conducting background is completely different from that of conductors in empty space, but the signals remain in the same order of magnitude. The SCR increases near the sending or receiving coils, but remains between 10^{-5} and 10^{-6}.

The absolute voltage change ΔV determines the signal-to-noise ratio (SNR) of the measurement system. It depends linearly on the excitation current I_{EXC} and the number of turns n_{EXC} and n_{REC} of the excitation and receiver coils. The above example yields $-3.9 \cdot 10^{-12} - j2 \cdot 10^{-8}$ V at 50 kHz with

$I_{\mathrm{EXC}} = 1$ A, $n_{\mathrm{EXC}} = 10$ and $n_{\mathrm{REC}} = 40$. As V_0 in (2) is proportional to ω, $\mathrm{Im}(\Delta V)$ increases with the square of the frequency. At 50 kHz, the imaginary part lies in the range of several nV. In a practical setting, the excitation current is limited by safety regulations for the maximum allowed specific absorption rate produced by the eddy currents. As it increases quadratically with the frequency, the maximum allowable current must decrease with the square of the frequency. At 50 kHz, excitation currents in the range of some tens of A are admissible. In our experiments, we applied maximum values of 20 $\mathrm{A_{rms}}$ so that $\mathrm{Im}(\Delta V)$ for the above example increases to $6 \cdot 10^{-7}$ V. As a conclusion, we can expect signals around 1 μV for a coaxial coil system with 250 mm distance and a spherical perturbation of 1 S/m with a diameter of 50 mm. Thinking of resolving conductivity changes of at least 10 mS/m (a reasonable upper limit for biological tissues) signals of 10 nV must be detected.

D. Application Example 2: Detection of Dia- and Paramagnetic Perturbations $(\chi_m \neq 0)$

Soft biological tissues and water are both diamagnetic materials with a magnetic susceptibility (χ_m) around $-10 \cdot 10^{-6}$ [13], [14].

The storage iron in the body is found in two iron-protein complexes, ferritin and hemosiderin, which possess paramagnetic conduct; thus, accumulation of iron in the liver produces a decrease of its diamagnetism. The iron concentration in a normal adult liver lies around 250 μg of Fe/g of wet liver tissue with a range of 50–500 μg/g being considered normal [14]. An iron content of more than 1 g in the liver is considered as hepatic iron overload (> 700 μg/g). In very strong iron overload, the liver can contain up to 14 g (9 mg/g of liver tissue) [13]. The magnetic susceptibility (χ_m) of hepatic tissue will be in the range $-9 \cdot 10^{-6}$ (normal) to $+5.2 \cdot 10^{-6}$ (overload) [13], [25].

The expected Re(SCR) for a cylinder of water $(\chi_m = -10 \cdot 10^{-6})$ with radius 25 mm, with a volume equal to the sphere used in the application example 1, is $-0.36 \cdot 10^{-6}$. For a normal liver sample, $(\chi_m = -9 \cdot 10^{-6})$ $\mathrm{Re(SCR)} = -0.32 \cdot 10^{-6}$ and for a strong overload, $(\chi_m = 5.2 \cdot 10^{-6})$ $\mathrm{Re(SCR)} = 0.19 \cdot 10^{-6}$.

Following the previous example, with a current of 20 $\mathrm{A_{rms}}$ and taking into account the diamagnetism of water, the expected signal is $\mathrm{Re}(\Delta V) = -2.3 \cdot 10^{-7}$ V.

This is in the same order of magnitude as the imaginary part due to the physiological conductivity, and shows that the contribution of permeability must be taken into account measuring at low frequencies. Also, the contribution of diamagnetism (permeability) produces a signal 4 orders of magnitude bigger than the contribution of the permittivity in the case of water at 50 kHz $(\varepsilon_r = 80)$.

Nevertheless, for biological tissue the strong increase of its permittivity when decreasing the frequency must be taken into account. As an example, the liver has a permittivity of $5.5 \cdot 10^4$ at 10 kHz and $5.0 \cdot 10^7$ at 10 Hz [1]. This effect can, at least partly, compensate the quadratic frequency term in (2).

E. Technical Requirements

1) SNR: Modern differential amplifiers with a spectral noise density ≤ 7 nV/sqrt(Hz) are commercially available.

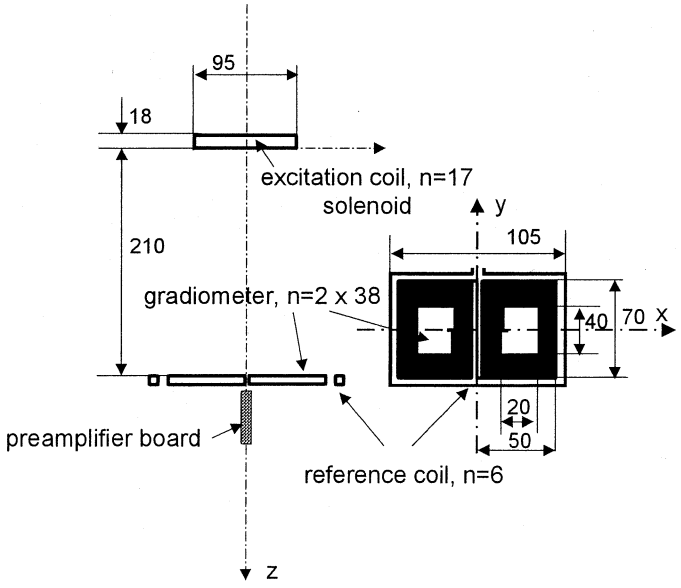

Fig. 3. Coil system consisting of excitation coil, reference coil and PGRAD. All measures in millimeters.

Custom-made amplifiers with less than 1 nV/sqrt(Hz) can be designed when employing several ultra-low-noise differential transistor pairs or whole differential amplifiers in parallel.

The desirable SNR of a MIS-system depends much on the application. Image reconstruction requires the highest SNR values of 40–60 dB. In less demanding cases 20 dB may be sufficient. Hence, taking into account a ΔV of 10 nV as estimated for application example 1, the noise voltage must remain below 1 $\mathrm{nV_{rms}}$. This means that, even with the best available amplifiers, the bandwidth must be kept below 1 Hz, which excludes applications with fast signal changes. However, during brain edema monitoring no fast changes are expected. Further improvement of the SNR can only be achieved with averaging, thus, further increasing the acquisition times.

2) Suggested Coil System: As the SCR of a coaxial coil system is very small the signal is below the quantization noise of most analog-to-digital converters. An appropriate design of the coil system can increase the SCR significantly. A simple approach is to subtract from the signal a voltage as close as possible to V_0 while maintaining ΔV approximately at the original level. This can be achieved easily with a gradiometer, i.e., two coils which are connected in counter-phase. In an ideally adjusted gradiometer the voltage induced in the absence of an object is zero because both halves of the coil experience the same magnetic flux.

In contrast to previous approaches [3], [26], [27], we introduced as receiver a planar gradiometer (Fig. 3). This coil system exhibits an antisymmetric sensitivity with respect to the z axis [7] and shall be referred to as "COIL-PGRAD." The reference coil REF is mounted on the same board (PCB) as the PGRAD, hence providing a mechanically robust and thermically well-coupled receiver.

3) Analysis of the Systematic Errors: As ΔV is extremely small it is susceptible to interference and drift. The most important sources for systematic errors in a COIL-PGRAD channel are as follows:

- moving well-conducting and/or ferromagnetic material near the object space;
- thermal drifts of the receiver's electrical properties;
- displacements of the receiver coil with respect to the excitation coil;
- phase-mismatch between the channels for reference coil and gradiometer.

Also, capacitive coupling between transmitter and receiver could be another important error if electrostatic screening is not adequate. There are two ways of avoiding this effect: the use of symmetric structures with differential amplifiers [with a high common mode rejection ratio (CMRR)] and the use of electrostatic shields connected to ground to reduce the coupling between parts at high voltage and the receivers. Both methods were implemented in the presented system.

We evaluated the errors as relative changes $\Delta V/V_0$ of the voltage due to artifacts. The individual contributions were then compared with a desired resolution limit of 10^{-7} which is the value which we could achieve in previous experiments.

Moving conducting or ferromagnetic parts in the surroundings of the transmitter cause a $|\mathrm{Re}(\Delta V/V_0)|$ in the same order of magnitude or even much bigger than $|\mathrm{Im}(\Delta V/V_0)|$. This occurs due to a violation of the condition for "weak perturbation," i.e., due to the very small penetration depth of the electromagnetic field in metals. Note that this case cannot be described correctly by (2). We define as indifference surface Γ_{IM} the set of all possible centers of a metallic sphere (radius r_M, conductivity σ_M) which causes a $|\mathrm{Im}(\Delta V/V_0)| = 10^{-7}$ when moved from infinity toward the coils. Analogously we define an indifference surface Γ_{RE} for the real part of the signal. Evidently, Γ_{IM} is relevant for the measurement of conductivity whereas Γ_{RE} is relevant for measurements of the magnetic permeability and permitivity. For estimating the allowable distance between a small conductor and the transceiver, we calculated the intersection curve between Γ_{IM} and the x–z plane (see Fig. 1). Analogously also Γ_{RE} was determined, which becomes important for the detection of susceptibility changes. Due to the invalidity of (2) for this case we applied the algorithm described in appendix A2 of [8]. The parameters of the model were: $r = 2$ cm, $\sigma = 3.7 \cdot 10^7$ S/m (Al), and $f = 150$ kHz.

In order to estimate the thermal drift, we modeled the PGRAD as a network of inductances (L), resistances (R) and capacitances (C), i. e. a LRC-network (Fig. 4) with: L_G, $L_G{}'$, coil inductances; C_G, $C_G{}'$, parallel capacitances due to mutual coupling between the windings and between the coils and the shield; R_G, $R_G{}'$, effective resistances of the coils; $V_{1,0}$, $V_{2,0}$, EMF induced in the coils. V_1 and V_2 cancel out mutually only if both coils are mechanically adjusted to receive the same magnetic flux and if the electrical parameters of both halves are identical. Inhomogeneous temperature changes in the PGRAD provoke a mismatch of the electrical parameters and of V_1 and V_2. Assuming a change of V_1 only by keeping the second gradiometer half at a perfectly constant temperature the $\Delta V/V_0$ due to a temperature difference ΔT is

$$\frac{\Delta V}{V_0} = \frac{1}{V_0}\left\{\frac{\partial V_1}{\partial V_{1,0}}\frac{dV_{1,0}}{dT} + \frac{\partial V_1}{\partial R}\frac{dR}{dT} + \frac{\partial V_1}{\partial L}\frac{dL}{dT} + \frac{\partial V_1}{\partial C}\frac{dC}{dT}\right\}\Delta T. \tag{3}$$

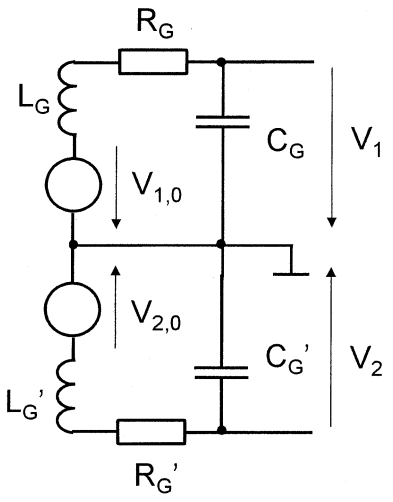

Fig. 4. Electrical model of the PGRAD.

The temperature coefficients of $V_{1,0}$, L and C include the thermal expansion coefficient of the conductors and, hence, the thermal change of the effective coil area. We evaluated (3) for a ΔT of 0.1 K between both halves of the PGRAD. The model parameters were: $R_G = 11\ \Omega$; $L = 106\ \mu$H; thermal expansion coefficient of Cu: $1.6 \cdot 10^{-5}$ K^{-1} [28]; thermal expansion coefficient of the PCB: $3.5 \cdot 10^{-5}$ K^{-1} [29]; ε of the PCB: 4.5 [29]; $d\varepsilon/(\varepsilon dT)$ of the PCB: 10^{-4} K^{-1} [30]; and $dR_G/(R_G dT)$: 0.004 K^{-1} [31]. The equivalent parallel capacitance C was 16 pF. This value was obtained by measuring the resonance frequency of the PGRAD.

A small lateral displacement Δx of the receiver coil with respect to the excitation coil leads to a change of the magnetic flux in both halves of the gradiometer. The resulting spurious $\Delta V/V_0$ is

$$\frac{\Delta V}{V_0} = \frac{1}{V_0}\frac{\partial \Delta V}{\partial x}\Delta x. \tag{4}$$

To estimate the effect of a displacement $(\partial \Delta V)/(\partial x)$ was calculated from the magnetic flux balance for the PGRAD before and after the displacement. The magnetic field distribution was calculated with the program described in [8]. The results were compared with experimental data when laterally displacing the gradiometer by 0.1 mm. Moreover, we measured the variation of the real and imaginary part of the gradiometer voltage by exposing the coil system to lateral vibrations with a frequency of 5 Hz and an amplitude of 1 mm.

A phase mismatch ϑ between the amplifiers of PGRAD and REF introduces spurious components (crosstalk) in the detected real and imaginary parts

$$\begin{aligned}\text{detected } \mathrm{Im(SCR)} &= \mathrm{Im(SCR)}\cos(\vartheta) \\ &\quad - \mathrm{Re(SCR)}\sin(\vartheta) \\ \text{detected } \mathrm{Re(SCR)} &= \mathrm{Im(SCR)}\sin(\vartheta) \\ &\quad + \mathrm{Re(SCR)}\cos(\vartheta).\end{aligned} \tag{5}$$

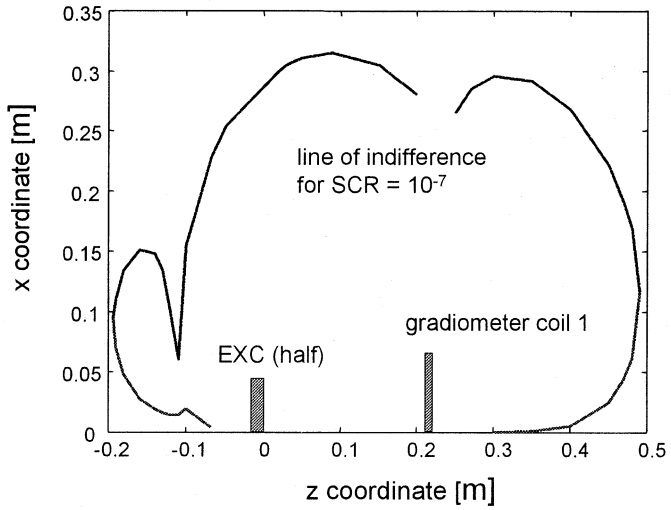

Fig. 5. Intersection of the indifference surface Γ_{IM} with the x–z plane for a SCR of 10^{-7}. Data are given for a 4-cm-diameter aluminum sphere and a frequency of 150 kHz.

F. Instrumentation

Two differential amplifiers (MAX 435) were mounted below the receiver board in the zone of minimal sensitivity. To avoid errors due to capacitive coupling, all coils (EXC, REF, and PGRAD) were electrostatically shielded. The signals were further amplified in two wideband amplifiers, the total gain being 698 (PGRAD) and 88 (REF). For each measurement point, 16 480 samples of both signals were sampled with a digital storage oscilloscope HP54520A (DSO) at 10 MS/s. Real and imaginary part of the PGRAD signal with respect to the reference voltage were calculated by digital coherent demodulation on a PC.

III. Results

With a previous version of the coil system shown in Fig. 3 the resulting SNR allows to resolve objects with a SCR of 10^{-7} [7], [8]. In [8], we demonstrated the feasibility of MIS for biological tissue in a frequency range of 30–500 kHz.

When using the MAX435 as preamplifier we obtained an equivalent noise voltage density at the amplifier input of $\sim 11\ \mathrm{nV}/\sqrt{\mathrm{Hz}}$, i.e., 1.4 times more than theoretically expected. Part of the excess may be due to interferences with external field sources. With an excitation current of 800 $\mathrm{mA_{PP}}$ the STD of the SCR was somewhat below 10^{-6} (without averaging). The cancellation factor $\mathrm{c_V}$ of the gradiometer changed from >1000 to about 150 when varying the frequency between 50 kHz and 1 MHz, thus providing satisfactory wideband operation.

A. Moving Well-Conducting Objects

Fig. 5 shows the intersection between the indifference surface Γ_{IM} and the x–z plane for $\mathrm{SCR} = 10^{-7}$. In the most sensitive zone (at $z = 0.08$ m), the allowable distance from the axis is somewhat above 0.3 m. When calculating Γ_{RE} the corresponding point is by a factor of 2.34 farther away, i.e., at about 0.7 m from the axis. $\mathrm{Re}(\Delta V/V_0)$ is 62 times larger than $\mathrm{Im}(\Delta V/V_0)$.

B. Thermal Drift

A ΔT of 1 K between both halves yields an $\mathrm{Im}(\Delta V/V_0)$ of $4.8 \cdot 10^{-7}$ at 100 kHz and a nearly linear increase with the frequency up to 1 MHz where $\mathrm{Im}(\Delta V/V_0)$ was $4.8 \cdot 10^{-6}$. The nearly linear increase with the frequency disappears when approaching the resonant frequency f_{res} (2.8 MHz) where $d\mathrm{Im}(\mathrm{SCR})/dT$ reaches a value as high as $5 \cdot 10^{-3}\ \mathrm{K}^{-1}$. $\mathrm{Im}(\Delta V/V_0)$ is essentially affected by dR_G/dT, contributing by 2–3 orders of magnitude more than dL/dT, dC/dT,and $dV_{1,0}/dT$. $\mathrm{Re}(\Delta V/V_0)$ is with $3.2 \cdot 10^{-5}$ (100 kHz) and $3.7 \cdot 10^{-5}$ (1 MHz) significantly larger than the imaginary part, the most important factors being $dV_{1,0}/dT$ and, to less extent, dL/dT and dC/dT.

C. Displacement of the Receiver Coil

The lateral shift of the PGRAD by 0.1 mm yields a calculated $\partial\mathrm{Re}(\Delta V/V_0)/\partial x$ of $-0.0113\ \mathrm{mm}^{-1}$ compared with $-0.0111\ \mathrm{mm}^{-1}$ measured. According to the simulation $\partial\mathrm{Im}(\Delta V/V_0)/\partial x$ is by c_V lower than $\partial\mathrm{Re}(\Delta V/V_0)/\partial x$. Without vibration the STD of the real and imaginary part of the voltage changes ΔV at the PGRAD were $3.9 \cdot 10^{-7}$ V and $3.8 \cdot 10^{-7}$ V, respectively. Under vibration, the $\mathrm{STD}(\mathrm{Im}(\Delta V))$ remained with $4.2 \cdot 10^{-7}$ V nearly constant and $\mathrm{STD}(\mathrm{Re}(\Delta V))$ increased to $3.5 \cdot 10^{-6}$ V.

IV. Discussion

A. Sensitivity Considerations

As demonstrated in previous publications [8], [17], [18], the presented magnetic induction technique renders possible the resolution of (patho-)physiological changes of both the electrical conductivity and the magnetic permeability in biological tissues. Whereas previous publications focus on either the conductive or the magnetic aspect of inductive measurements in tissues, this article aims at a synthesis of both concepts by discussing two different applications with one and the same measurement system.

Although based on several simplistic assumptions, (2) reflects this synthesis in a quite intuitive way by relating the sensitivities of a coaxial coil-coil system to the different PEP and the most important measurement parameters. It allows the estimation of the expected SCR and reveals how to separate the different contributions by selecting appropriate frequency bands and synchronous demodulation.

However, bearing in mind the complexity of the general electromagnetic theory behind the problem [see (1)] the limits of validity of (2) must be stressed. The two most important limitations are as follows:

1) equation (2) is only valid in case of weak perturbation as defined in the introduction;
2) it has been derived for an isolated object in the empty space.

Limitation 2 becomes important when studying target objects (organs) which are embedded in a surrounding conducting and/or diamagnetic background.

When focussing on the magnetic term (measurement of χ_m), the total magnetization in the volume Ω can be obtained by

linear superposition of the weighted contribution of the magnetization in individual volume elements. The total response is then obtained by spatial convolution of the distribution of magnetic moments with the 3-D sensitivity map of the measuring system. The sensitivity map can be calculated with (2), when discretizing the space into small volume elements in cylinder coordinates. This means that the reconstruction of images from different projections is, in principle, possible with classical deconvolution techniques or simply with weighted backprojection like in X-ray CT.

This is not true, however, for the conductive part of the sensitivity relation. As the underlying electromagnetic phenomenon is that of eddy currents, the sensitivity map cannot be derived by linearly superposing the contributions of isolated volume elements when dealing with inhomogeneous conductors. Although several authors claimed the applicability of backprojection, this technique cannot be valid, except in some exceptional cases [19]. In many biomedical situations (2) and other solutions for isolated conducting objects in the empty space [7], [8], [10] loose their validity and the complete eddy current problem has to be solved by numerical methods. However, as shown in [19], the expected sensitivities remain in the same order of magnitude as those calculated with (2). Hence, with some caution, the obtained data can still be used for the estimation of the system requirements, such as the SNR.

B. Measurement System and Systematic Errors

We analyzed different systematic errors. Drifts of the excitation current have been excluded from the analysis as they can be compensated easily by calculating the ratio between the signals in gradiometer and reference coil.

1) Moving Well-Conducting Objects: Moving conductors mimic a change of both κ and μ in the region of interest, unless located far outside the indifference surface. An Al-sphere with a radius of 2 cm located ~40 cm away from the receiver yields an $\mathrm{Im}(\Delta V/V_0)$ which is close to the desired resolution of 10^{-7} for conductive perturbations. It produces the same Im(SCR) as a nonmagnetic sphere with the same radius and 0.02 S/m at $x = 0.025$ m, $z = 0.18$ m. Assuming a desired resolution of 0.01 S/m small moving metallic parts should remain even farther away.

The real part $\mathrm{Re}(\Delta V/V_0)$ is much bigger than the imaginary part, in our example by a factor of 62. Hence, moving metallic objects can be distinguished relatively easily from biological material the Re(SCR) of which is usually lower than Im(SCR) at frequencies below 1 MHz.

When measuring pathophysiological changes of the magnetic permeability [Re(SCR) down to 10^{-7}] metallic moving objects must be kept even significantly farther away from the system than for conductivity measurements (in our example by a factor of 2.34). In this paper, we examined only the influence of a nonmagnetic perturbation, the situation is expected to deteriorate further if moving magnetic materials exist in the surroundings of the sensor system.

2) Thermal Drift: $\Delta V/V_0$ changes with the temperature, whereby the real part is again much more affected than the imaginary part if the frequency is sufficiently below f_{res}. At 150 kHz, a change of the temperature difference between both gradiometer coils by 0.15 K introduces an $\mathrm{Im}(\Delta V/V_0)$ of 10^{-7}, i.e. the desired resolution limit. In the presented PGRAD, $d\mathrm{Im}(\Delta V/V_0)/dT$ increases linearly with the frequency up to 1 MHz. As Im(SCR) of a biological conductor also increases linearly with the frequency, the relative error remains constant. The effect gets worse with increasing resistance R_G, making the latter an important design parameter for the PGRAD. The error can be reduced by proper coil design of the PGRAD (good thermal coupling between coils, thermal insulation from the environment, low R_G, high f_{res}).

Re(SCR) is much more affected by a thermal mismatch of the gradiometer halves than the imaginary part. At 150 kHz, a temperature difference of 0.003 K can already introduce an error in the range of the desired resolution of 10^{-7}. In contrast to the imaginary part, the thermal coefficient of the real part does not change all too much with the frequency, maintaining the error at an approximately constant level also at very low frequencies. The main reason for this behavior is the strong dependence of Re(SCR) on dV_0/dT which is due to the thermal expansion of the printed board and, hence, does not depend on the frequency.

3) Displacement of the Receiver Coil: Our analysis refers to lateral displacements of the gradiometer because these are regarded as the most severe case. Translations in direction y and z as well as rotations about the z and x axis do not introduce signal changes due to symmetry considerations. However, rotations about the y axis can lead to similar effects as lateral displacements in direction x. $\mathrm{Im}(\Delta V/V_0)$ is theoretically by $1/\psi$ lower than $\mathrm{Re}(\Delta V/V_0)$, ψ denoting the phase mismatch between both halves of the gradiometer. Thus, Im(SCR) remains essentially unaffected by lateral vibrations if ψ is small enough. Assuming a displacement by 0.01 mm and a ψ of 10^{-3} rad (0.057°) $\mathrm{Im}(\Delta V/V_0)$ is $1.2 \cdot 10^{-7}$, i.e., close to the desired resolution limit. This desirable property diminishes with increasing phase mismatch ϑ between REF and PGRAD amplifiers as then, according to (5), $\mathrm{Re}(\Delta V/V_0)$ is projected into the imaginary axis.

In contrast to the imaginary part, the real part of the SCR is very sensitive to mechanical shifts of the receiver with respect to the EXC. A displacement by 0.01 mm and a Ψ of 10^{-3} yields a $\mathrm{Re}(\Delta V/V_0)$ of $1.2 \cdot 10^{-4}$. In order to reduce, this spurious signal to the desired level of 10^{-7}, the lateral movement must not exceed 10 μm, a condition which is very difficult to meet in practice.

4) Phase Mismatch Between the Channels: A phase mismatch ϑ between the amplifiers in the REF and PGRAD channels does not produce a distortion of Im(SCR) by itself. Its effect is seen in combination with an important real part of the signal, which may stem from strong conductors outside the object space. This error is calibrable by measuring the SCR of a weak conductor and correcting ϑ by solving (5).

When measuring dia- or paramagnetic effects at high frequencies, Im(SCR) can become considerably higher than Re(SCR). In this case also, care must be taken in order not to project imaginary components into the real axis due to a phase mismatch ϑ. If the imaginary part is not of interest, it is, hence, recommendable to carry out the measurements at very low frequencies, where the imaginary part becomes negligible (e.g., at 5 kHz) and, as a side effect, usually also ϑ becomes negligible.

Clearly, in this case, the SNR of the system must be increased, e.g., by increasing the number of turns of both the EXC and the PGRAD.

5) Overall Error: It appears possible to keep the sum of all systematic errors of the imaginary part of the SCR in the range of 10^{-7}. However, lower values (as still desirable) may not be reached with a system without magnetic shielding and without active control of the thermal mismatch between the gradiometer coils. In contrast, the real part may be corrupted heavily by all discussed kinds of errors. Evaluation of the real part for the extraction of the imaginary part of κ appears more difficult due to its low level at low frequencies, also considering the increase of the permittivity at very low frequencies.

In the absence of fast thermal drifts and moving metallic parts, errors due to thermal drift in the receiver are calibrable by repeated data acquisition with the empty system between individual measurements.

A possible way of separating system drifts and temporal changes of the conductivity data is the exploitation of the multifrequency information, e.g. in terms of the Cole-Cole parameters [32], [33]. If only the morphological characteristics of the conductivity spectra are evaluated ("parametric imaging," see for a review, e.g., [34]), errors in the absolute values do not affect the results strongly. A prerequisite is that the systematic errors exhibit a stable or at least calibrable frequency dependence. This condition is not self-evident and should be investigated carefully in future work.

The effect of displacements of the receiver does, at least theoretically, not depend on the frequency. Thus, it can be separated entirely by measurements at low frequencies, where the other contributions disappear.

Due to their considerable real part, all important systematic errors can be detected but not entirely separated. They can be filtered out if their frequency content is significantly different from that of the desired signal. If this is not the case a correction of the imaginary part by correlation with the real part is possible if *a priori* knowledge about the perturbations is available.

As Re(SCR) is very sensitive to all of the discussed errors, measurement of the magnetic permeability is difficult in motionless objects. However, if it is possible to move the object periodically (mechanical chopping), the signal can be extracted more easily by correlation analysis. As has been demonstrated in previous experiments [17], [18], this technique allows to measure changes of Re(SCR) down to $2 \cdot 10^{-7}$, even with an unshielded system.

Calibration without removing the object under measurement (on-line monitoring) may become possible by coupling a calibration field into the receiver coil system in such a way, that the sensitivity for the object is negligible. This can be achieved with a symmetrically arranged small calibration coil directly on the receiver board.

V. Conclusion

MIS offers the possibility of measuring physiological changes of the complex conductivity and of the magnetic permeability. However, due to the extremely low signal levels, the data can be corrupted by various disturbing effects. The real part of the signal is always much more affected by artifacts than the imaginary part. For instance, an aluminum sphere moving near the object space introduces a spurious $\Delta V/V_0$ the real part of which is by a factor of 62 larger than the imaginary part. A thermal mismatch of 0.15 K between both gradiometer halves introduces an $\mathrm{Im}(\Delta V/V_0)$ of 10^{-7} at 150 kHz whereas the change in the real part is by a factor of 50 larger. $\mathrm{Re}(\Delta V/V_0)$ caused by small lateral displacements of the receiver can be by a factor of more than 1000 (cancellation factor of the PGRAD) higher than the imaginary part which does not exceed 10^{-7} for a displacement of 10 μm. It appears possible to keep the sum of all systematic errors of the imaginary part of the SCR in the range of 10^{-7}. This error allows the resolution of 10^{-3} S/m or better in medium-sized (some cm of radius) biological target objects, provided the amplifier noise does not exceed 1 nV/$\sqrt{\text{Hz}}$. Above 100 kHz, measurements of the real part σ of the conductivity are considerably less prone to drifts than measurements of the permeability μ. However, long-term measurements without repetitive calibration of the system may provide poor reliability of the data.

In conclusion, further investigations shall concentrate on both, the exploitation of multifrequency information as well as the development of appropriate calibration techniques.

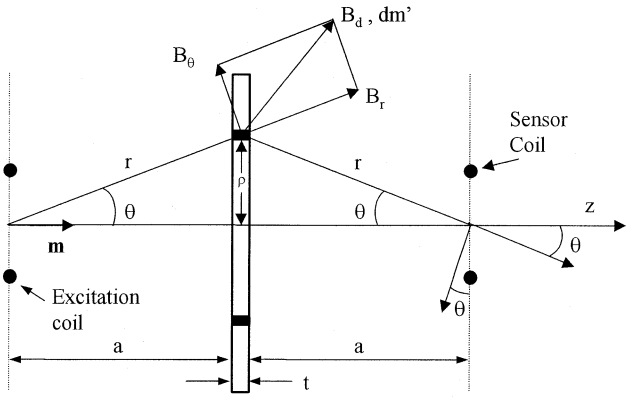

Fig. 6. Model of the electromagnetic coupling between a cylindrical sample and a coil system.

Appendix I
Derivation of the Permeability Contribution in (2)

Consider two coils positioned coaxially (Fig. 6) and spaced by a distance $2a$. A sinusoidal current, of angular frequency ω, in the excitation coil produces a magnetic field B_0 that is measured at the receiver coil. Both coils are supposed to have a small radius with respect to their distance and are, thus, modeled as magnetic dipoles. Suppose a circular disc of radius R, thickness t ($t \ll 2a$), conductivity $\kappa = \sigma + j\omega\varepsilon_0\varepsilon_r$, and relative permeability μ_r, placed coaxially and centrally between the coils. The magnetic field B_0 will induce eddy currents and magnetization in the disc. Eddy currents produce a perturbation ΔB_e [21] of B_0. Moreover, the magnetic field magnetizes the disc,

thus causing an additional perturbation ΔB_m. The magnitude of the excitation field B_d in the plane of the disc is given by (1) (see Fig. 6), where m is the dipole moment of the excitation coil

$$B_d = \frac{\mu_0 m (4a^2+\rho^2)^{\frac{1}{2}}}{4\pi(\rho^2+a^2)^2}. \tag{6}$$

This field induces a dipole dm in the differential element of volume in ρ, $\rho+d\rho$ and φ, $\varphi+d\varphi$; the magnitude of this dipole is given by

$$dm = \left[\frac{(\mu_r-1)mt(4a^2+\rho^2)^{\frac{1}{2}}\rho}{4\pi(\rho^2+a^2)^2\mu_r}\right] d_\rho d_\varphi. \tag{7}$$

Every dipole produces a differential perturbation field in the sensor coil. After integration over the entire disc volume the total relative perturbation due to magnetization in the sensing coil (only z component) is

$$\frac{\Delta B_m}{B_0} = \frac{\left[a^3 t R^2 (8a^2-R^2)(\mu_r-1)\right]}{\left[2\mu_r(a^2+R^2)^4\right]}. \tag{8}$$

For a μ_r close to 1, the term $(\mu_r-1)/\mu_r$ can be approximated by $(\mu_r-1)=\Delta\mu_r$. This approximation is valid for paramagnetic and diamagnetic materials.

Above 60 K and low frequency, the complex part of the magnetic susceptibility is essentially zero for paramagnetic material [35]. Therefore, the complex behavior of μ_r is not considered for biological tissues at normal temperatures. By definition $\mu_r = 1+\chi_m$ and $\chi_m = \mu_0 \mathrm{Nm}^2/3\mathrm{KT}$ (weak magnetism), where μ_0 is the permeability of the free space, N the number of magnetic dipoles per unit volume, m the magnetic moment of each dipole, K the Boltzman constant, and T the absolute temperature.

Appendix II
Analysis of the Systematic Errors

A. Parameter Mismatch of the Gradiometer Coils

This analysis refers to the equivalent LRC-network as depicted in Fig. 4. The voltages V_1 and V_2 experience a phase shift with respect to the EMF's $V_{1,0}$ and $V_{2,0}$ induced in the coils. Imperfect matching of the electrical parameters yields a phase mismatch ψ between V_1 and V_2. The corresponding difference voltage ΔV is calculated according to

$$\begin{aligned} |\Delta V| &= \sqrt{(|V_1|-|V_2|\cos(\psi))^2+(|V_2|\sin(\psi))^2} \\ \varphi &= a\tan\left(\frac{|V_2|\sin(\psi)}{|V_1|-|V_2|\cos(\psi)}\right) \end{aligned} \tag{9}$$

whereby φ is the phase angle of ΔV with respect to V_1. Obviously ΔV cannot be cancelled completely just by adjusting the magnitude of V_2 as it is the case by a lateral displacement of the gradiometer. Setting $|V_2| = k|V_1|$ a minimum value of ΔV is obtained for $k=\cos(\psi)$. With this definition the real and imaginary part of ΔV can be expressed as

$$\begin{aligned} \mathrm{Re}(\Delta V) &= |V_1|(1-k\cos(\psi)) \\ \mathrm{Im}(\Delta V) &= |V_1| k \sin(\psi). \end{aligned} \tag{10}$$

For $\psi \ll 1$ $|\Delta V|$ reaches a minimum value of $V_1\psi$ if $k=1$ and $\varphi=\pi/2$. Hence, V_1 cannot be suppressed by more than a factor $1/\psi$ and the minimum ΔV is in quadrature with V_1. The term $1/\psi$ equals the maximum possible cancellation factor. Ψ, V_1 and V_2 depend on the parameters of the LRC-network in Fig. 4.

B. Thermal Mismatch of the Gradiometer Coils

The electrical parameters of the model depend on the temperature T. Assuming a perfect matching at $\Delta T=0$, V_1 equals V_2 in the adjusted gradiometer. A temperature change ΔT in coil 1 provokes the following:

- change ΔR due to the temperature coefficient of copper;
- change ΔL due to a thermal expansion of the conductors;
- change ΔC due to a thermal expansion of the conductors and the temperature coefficient of the dielectric permittivity;
- change $\Delta V_{1,0}$ due to a change of the thermal expansion of effective coil area and, hence, of the magnetic flux.

A spurious change $\Delta V/V_0$ can be calculated according to

$$\frac{\Delta V}{V_0} = \frac{1}{V_1}\frac{dV_1}{dT}\Delta T. \tag{11}$$

In terms of the model parameters, dV_1/dT can be expressed as

$$\begin{aligned} \frac{dV_1}{dT} &= \frac{d}{dT}\left(\frac{V_{1,0}}{1-\omega^2 LC - j\omega RC}\right) \\ &= \frac{d}{dT}\left(\frac{V_{1,0}(1-\omega^2 LC + j\omega RC)}{(1-\omega^2 LC)^2+(\omega RC)^2}\right). \end{aligned} \tag{12}$$

Decomposition into real and imaginary part gives

$$\begin{aligned} \frac{d\mathrm{Re}(V_1)}{dT} &= \frac{\partial \mathrm{Re}(V_1)}{\partial V_{1,0}}\frac{dV_{1,0}}{dT} + \frac{\partial \mathrm{Re}(V_1)}{\partial R}\frac{dR}{dT} \\ &\quad + \frac{\partial \mathrm{Re}(V_1)}{\partial L}\frac{dL}{dT} + \frac{\partial \mathrm{Re}(V_1)}{\partial C}\frac{dC}{dT} \\ \frac{d\mathrm{Im}(V_1)}{dT} &= \frac{\partial \mathrm{Im}(V_1)}{\partial V_{1,0}}\frac{dV_{1,0}}{dT} + \frac{\partial \mathrm{Im}(V_1)}{\partial R}\frac{dR}{dT} \\ &\quad + \frac{\partial \mathrm{Im}(V_1)}{\partial L}\frac{dL}{dT} + \frac{\partial \mathrm{Im}(V_1)}{\partial C}\frac{dC}{dT}. \end{aligned} \tag{13}$$

The calculation of the partial derivatives $d\mathrm{Re}(V_1)/d(.)$ and $d\mathrm{Im}(V_1)/d(.)$ of (13) was carried out automatically with the symbolic toolbox of MATLAB.

The thermal coefficient of the resistance $dR/(RdT)$ of copper was looked up in the literature. The temperature coefficient of L was calculated for a quadratic coil with n turns and a medium edge length of $l$as follows: The unperturbed inductance is given by $L_0 = Dl^2n^2$, D being a geometrical constant. Hence

$$\frac{dL}{dT} = 2Dn^2 l\frac{dl}{dT} = \frac{2L_0}{l}\frac{dl}{dT} \tag{14}$$

whereby $dl/(ldT)$ represents the thermal expansion coefficient of the conductor. $dV_{1,0}/dT$ is derived from the change of the mutual inductance M between EXC and gradiometer coil

$$\begin{aligned} V_{1,0} &= -j\omega I_{\mathrm{EXC}} M \\ \frac{dV_{1,0}}{dT} &= -j\omega I_{\mathrm{EXC}}\frac{dM}{dT} = \frac{dM}{dT}\frac{V_{1,0}}{M}. \end{aligned} \tag{15}$$

Since at a constant number of turns M is proportional to L, one can also write

$$\frac{dV_{1,0}}{dT} = \frac{dL}{dT}\frac{V_{1,0}}{L} = \frac{2L_0V_{1,0}}{l}\frac{dl}{dT}. \tag{16}$$

The term dC/dT is much more complicated to estimate. In the simplest approach, we assume C to be essentially determined by the capacitance between the individual windings, thus neglecting the shield. The capacitance is $C = cl_{\text{eff}}$, with l_{eff} some effective length of the coil conductor and $c$the per length capacitance between two parallel infinitely long copper strips. For dC/dT, we obtain

$$\frac{dC}{dT} = l_{eff}\frac{dc}{dT} = \frac{dc}{dT}\frac{C}{c}. \tag{17}$$

Since l_{eff} does not appear in the final analysis, it needs not be specified. $c$is given by [36]

$$c = \frac{\pi\varepsilon}{\ln\left(\frac{a}{b}+1\right)} \tag{18}$$

whereby a is the distance between the center lines of the strips and b is the sum of width and height of one strip. ε is the permittivity of the medium. The temperature coefficient of c is obtained by

$$\frac{dc}{dT} = \frac{c}{\varepsilon}\frac{d\varepsilon}{dT} - \frac{c^2}{\pi\varepsilon\left(\frac{a}{b}+1\right)}\frac{1}{b}\frac{da}{dT} + \frac{c^2}{\pi\varepsilon\left(\frac{a}{b}+1\right)}\frac{a}{b^2}\frac{db}{dT}. \tag{19}$$

da/dt is determined by the thermal expansion coefficient of Cu and of the PCB whereas db/dT is essentially determined by the expansion coefficient of Cu.

C. Lateral Receiver Displacement

For evaluating (5) the derivative $d\Delta V/dx$ is required, ΔV being the voltage difference $V_1 - V_2$. V_1 and V_2 are calculated from the magnetic flux Φ_1 and Φ_2 in the coils 1 and 2 of the gradiometer according to

$$V_1 = -j\omega\Phi_1; \quad V_2 = -j\omega\Phi_2\exp(j\psi). \tag{20}$$

With the gradiometer adjusted $V_1 = V_2 = V_0$. Assume that the magnetic induction B varies only in direction x so as to exhibit a maximum in the center of the gradiometer. A displacement dx produces a change of the magnetic flux $d\Phi$ in coil 1 according to

$$d\Phi = A\left(B(x_2) - B(x_1)\right)dx \tag{21}$$

with A a geometrical factor and x_1 and x_2 the x-coordinates of the inner and outer border of the rectangular coil. The shift provokes a decrease of the flux in coil 1 and an equal increase in coil 2 which leads to a differential voltage change dV according to

$$V_1 = V_0 - \frac{dV}{2}; \quad V_2 = V_0 + \frac{dV}{2}$$
$$dV = j\omega d\Phi. \tag{22}$$

With the definition of k [see (10)] and substituting (20) and (21) into (22), one obtains

$$dk = \frac{dV}{V_0} = \frac{2A\left(B(x_2) - B(x_1)\right)}{A\int_{x1}^{x2} B dx}dx$$
$$\frac{dk}{dx} = 2\frac{B(x_2) - B(x_1)}{\int_{x1}^{x2} B dx}. \tag{23}$$

Differentiation of (10) with respect to x yields

$$\frac{d\text{Re}\left(\frac{\Delta V}{V_0}\right)}{dk}\frac{dk}{dx} = -\cos(\psi)\frac{dk}{dx}$$
$$\frac{d\text{Im}\left(\frac{\Delta V}{V_0}\right)}{dk}\frac{dk}{dx} = \sin(\psi)\frac{dk}{dx}. \tag{24}$$

For a small phase mismatch $\psi \ll 1$ and assuming a small lateral displacement Δx, $\Delta V/V_0$ can be expressed as

$$\text{Re}\left(\frac{\Delta V}{V_0}\right) = -\frac{dk}{dx}\Delta x$$
$$\text{Im}\left(\frac{\Delta V}{V_0}\right) = \psi\frac{dk}{dx}\Delta x. \tag{25}$$

Equation (25) shows that the imaginary part is by the factor $1/\Psi$ lower than that of the real part.

REFERENCES

[1] J. R. Bourne (Ed.), "Bioelectrical impedance techniques in medicine," *Crit. Rev. Biomed. Eng.*, vol. 24, 1996.

[2] S. Fujita, T. Ueda, and M. Yagi, "Detection of experimental and clinical brain edema using an electrical impedance method," *J. Neurosurg.*, vol. 37, pp. 156–163, 1972.

[3] J. Netz, E. Forner, and S. Haggemann, "Contactless impedance measurements by magnetic induction—a possible method for investigation of brain impedance," *Physiol. Meas.*, vol. 14, pp. 463–471, 1993.

[4] D. Murphy, P. Burton, R. Coombs, L. Tarassenko, and P. Rolfe, "Impedance imaging in the newborn," *Clin. Phys. Physiol. Meas.*, vol. 8, no. Suppl. A, pp. 131–140, 1987.

[5] L. Tarassenko and P. Rolfe, "Imaging spatial distribution of resistivity: an alternative approach," *Electron. Lett.*, vol. 20, pp. 29–33, 1984.

[6] D. Holder, "Opportunities for EIT in the nervous system," in *Clinical and Physiological Applications of Electrical Impedance Tomography*, D. Holder, Ed. London, U.K.: UCL Press, 1993.

[7] J. Rosell, R. Casañas, and H. Scharfetter, "Sensitivity maps and system requirements for Magnetic induction tomography using a planar gradiometer," *Physiol. Meas.*, vol. 22, pp. 121–130, 2001.

[8] H. Scharfetter, H. K. Lackner, and J. Rosell, "Magnetic induction tomography: hardware for multi-frequency measurements in biological tissues," *Physiol. Meas.*, vol. 22, pp. 131–146, 2001.

[9] S. Al-Zeibak and H. N. Saunders, "A feasibility study of *in vivo* electromagnetic imaging," *Phys. Med. Biol.*, vol. 38, pp. 151–160, 1993.

[10] A. V. Korjenevsky and V. A. Cherepenin, "Progress in realization of magnetic induction tomography," *Ann. N.Y. Acad. Sci.*, vol. 873, pp. 346–352, 1999.

[11] H. P. Kao, E. Shwedyk, and E. R. Cardoso, "Measurement of canine cerebral oedema using vector impedance methods," *Neurol. Res.*, vol. 13, pp. 233–236, 1991.

[12] H. P. Kao, E. R. Cardoso, and E. Shwedyk, "Correlation of permittivity and water content during cerebral edema," *IEEE Trans. Biomed. Eng.*, vol. 46, pp. 1121–1128, Sept. 1999.

[13] J. H. Bauman and R. W. Hoffman, "Magnetic suceptibility meter for *in vivo* estimation of hepatic iron stores," *IEEE Trans. Biomed. Eng.*, vol. BME-14, pp. 239–243, Oct. 1967.

[14] D. N. Paulson, R. L. Fagally, and R. M. Toussaint, "Biomagnetic susceptometer with squid instrumentation," *IEEE Trans. Magn.*, vol. 27, pp. 3249–3252, Sept. 1991.

[15] G. M. Brittenham, D. E. Farrell, J. W. Harris, E. S. Feldman, E. H. Danish, W. A. Muir, J. H. Tripp, and E. M. Bellon, "Magnetic-susceptibility measurement of human iron stores," *New Eng. J. Med.*, vol. 307, pp. 1671–1675, 1982.
[16] H. L. Bonkovsky, R. B. Rubin, E. E. Cable, A. Davidoff, D. H. Pels Rijcken, and D. D. Stark, "Hepatic iron concentration: noninvasive estimation by means of MR imaging techniques," *Radiol.*, vol. 212, pp. 227–234, 1999.
[17] R. Casañas, H. Scharfetter, A. Altes, and J. Rosell, "Magnetic induction system for noninvasive measurement of susceptibility and conductivity of biological tissues," in *Proc. XI ICEBI*, 2001, pp. 623–626.
[18] R. Casañas, H. Scharfetter, A. Altes, A. Remacha, P. Sarda, J. Sierra, and J. Rosell, "*In-vitro* measurement of iron concentration in human hepatic tissue by magnetic induction methods," in *Proc. 23rd Annu. Int. Conf. IEEE EMBS*, 2001, Paper #951 (CD).
[19] H. Scharfetter, P. Riu, M. Populo, and J. Rosell, "Sensitivity maps for low-contrast perturbations within conducting background in magnetic induction tomography (MIT)," *Physiol. Meas.*, vol. 23, pp. 195–202, 2002.
[20] J. R. Mortarelli, "A generalitation of the Geselowitz relationship useful in impedance plethysmography field calculations," *IEEE Trans. Biomed. Eng.*, vol. BME-27, pp. 665–667, Nov. 1980.
[21] H. Griffiths, W. R. Stewart, and W. Gough, "Magnetic induction tomography. A measuring system for biological tissues," *Ann. N.Y. Acad. Sci.*, vol. 873, pp. 335–345, 1999.
[22] M. Osypka and E. Gersing, "Tissue impedance spectra and the appropriate frequencies for EIT," *Physiol. Meas.*, vol. 16, no. 3 Suppl A, pp. A49–A55, 1995.
[23] B. Rigaud, L. Hamzaoui, and N. Chauveau *et al.*, "Tissue characterization by impedance: a multifrequency approach," *Physiol. Meas.*, vol. 15, pp. A13–A20, 1994.
[24] B. Rigaud, L. Hamzaoui, M. R. Frikha, N. Chauveau, and J. P. Morucci, "*In vitro* tissue characterization and modeling using electrical impedance measurements in the 100 Hz–10 MHz frequency range," *Physiol. Meas.*, vol. 16, no. 3 Suppl. A, pp. A15–A28, 1995.
[25] J. H. Bauman and J. W. Harris, "Estimation of hepatic iron stores by *in vivo* measurement of magnetic susceptibility," *J. Lab. Clin. Med.*, vol. 70, pp. 246–257, 1967.
[26] P. P. Tarjan and R. McFee, "Electrodeless measurements of the effective resistivity of the human torso and head by magnetic induction," *IEEE Trans. Biomed. Eng.*, vol. 15, pp. 266–278, Oct. 1968.
[27] H. Scharfetter, W. Ninaus, B. Puswald, G. I. Petrova, D. Kovachev, and H. Hutten, "Inductively coupled wideband transceiver for bioimpedance spectroscopy (IBIS)," *Ann. N.Y. Acad. Sci.*, vol. 873, pp. 322–334, 1999.
[28] T. Knight. (1994) Material Constants. [Online]. Available: http://www.ai.mit.edu/people/tk/tks/copper.html
[29] C. F. Coombs, *Printed Circuits Handbook*, 3rd ed. New York: McGraw-Hill, 1988.
[30] R. Kotte, E. Gockenbach, and H. Borsi. About the influence of the temperature on the dielectric properties of heat-resistant cast resins. presented at *Proc. 12th Int. Symp. High Voltage Engineering (ISH)*,. [Online]. Available: http://sun1.rrzn.uni-hannover.de/nhmasche/PDF/kotte_ish_01_2.pdf
[31] American Metal Market Llc. (2002, April) Electrical Conductivity of Metals.. [Online]. Available: http://www.amm.com/ref/conduct.htm
[32] K. S. Cole and R. H. Cole, "Dispersion and absorption in dielectrics. I. Alternating current characteristics," *J. Chem. Phys.*, vol. 9, pp. 341–351, 1941.
[33] S. Gabriel, R. W. Lau, and C. Gabriel, "The dielectric properties of biological tissues: III. Parametric models for the dielectric spectrum of tissues," *Phys. Med. Biol.*, vol. 41, pp. 2271–2293, 1996.
[34] J. P. Morucci and P. M. Marsili, "Bioelectrical impedance techniques in medicine. Part III: impedance imaging. Second section: reconstruction algorithms," *Crit. Rev. Biomed. Eng.*, vol. 24, pp. 599–654, 1996.
[35] P. D. Allen, T. G. St. Pierre, W. Chua-anusorn, V. Strom, and K. V. Rao, "Low-frecuency low-field magnetic susceptibility of ferritin and hemosiderin," *Biochimica et Biophysica Acta*, vol. 1500, pp. 186–196, 2000.
[36] R. Pallás Areny and J. G. Webster, *Analog Signal Processing*. New York: Wiley, 1999.

Hermann Scharfetter was born in Leoben, Austria, in June 1966. He received the M.Sc. and Ph.D. degrees in electrical engineering 1990 and 1995, respectively, both from the Graz University of Technology, Graz, Austria.

He was habilitated for "Biomedical Engineering" in 2000 and is currently Associate Professor at the Institute for Biomedical Engineering at the Graz University of Technology. His current research interest is focused upon noninvasive diagnostic methods based on the passive electrical properties of tissue, especially impedance spectroscopy, electromagnetic modeling, and magnetic induction tomography/spectroscopy.

Roberto Casañas received the Licentiate degree in physics from the Central University of Venezuela, Caracas, in 1984. He is currently working towards the Ph.D. degree in the Electronic Department in the Polytechnic University of Catalunya, Barcelona, Spain.

Since 1988, he has been with the Central University of Venezuela, where he is Professor in the Physical, Chemistry, and Mathematical Department in the Medical School. His main research interests are magnetic induction spectroscopy and electrical bioimpedance spectroscopy.

Javier Rosell was born in Barcelona, Spain, in June 1959. He received the Ingeniero de Telecomunicación and Doctor Ingeniero de Telecomunicación degrees in 1983 and 1989, respectively, both from the Polytechnic University of Catalunya (UPC), Barcelona, Spain.

He is currently Professor in the Department of Electronic Engineering and in the Biomedical Research Center at the UPC. His current research interest is focused on noninvasive measurement methods in the medical and biological fields, in particular, based on electrical impedance spectroscopy.